Phase diagram of a dusty plasma

H. C. Lee[1] and B. Rosenstein[2]

[1]*Department of Physics, National Central University, Chungli, Taiwan 320, Republic of China*
[2]*Department of Physics, National Tsing-Hua University, Hsinchu, Taiwan, Republic of China*

We show that dipole-dipole interactions induced by gravitational force and possibly ion-stream drag force give rise to stable triangular and oriented cubic crystalline structures recently observed in a dusty plasma, as opposed to only unoriented cubic close-packed structures usually expected of Wigner crystals. In certain cases the dipole interaction may flatten the crystal significantly. We calculate the phase diagrams of the crystals and analyze and explain some of their features. [S1063-651X(97)09305-7]

INTRODUCTION

Wigner crystallization of particles that repel each other has recently attracted the attention of both theoreticians and experimentalists. It differs significantly from the usual crystallization caused by a force that has both attractive and repulsive ("hard-core") components and hence provides an inherent scale that practically fixes the lattice spacing and the density of the crystal. In Wigner crystals density can vary. Recently, Wigner-type stable crystalline structures of dust particles in a plasma have been experimentally observed [1–6]. This opens the way for the study of the dynamical properties of crystals and their melting at the mesoscopic level using simple optical microscopy. These structures owe their surprising stability in the highly volatile plasma environment to the very effective charging of the dust particles, such that Coulomb interactions between the particles are in the so-called strong-coupling regime, where they dominate over the thermal motion of the particles. This phenomenon was predicted by [7].

The observed crystalline structures have two unexpected features: (i) the breaking of three-dimensional rotational symmetry and (ii) a preponderance of triangular structure. Specifically, a vertically aligned hexagonal lattice, which is far from being close packed, was observed in all three-dimensional samples together with triangular hexagonal-close-packed (hcp) and *oriented* cubic-close-packed fcc and bcc lattices with a distinguished vertical direction [1,5,6]. In contrast, it is well known that three-dimensional Wigner crystals with screened or unscreened Coulomb interactions have only two stable solid phases: an unoriented close-packed fcc and a bcc [8].

Gravity is an obvious source of the asymmetry. Another possible source is the drag force exerted on the dust particles by the ion stream in the plasma [9]. Recent Monte Carlo simulations of limit-size [10] and two-layer [11] systems that took into account the effects of gravity and ion stream demonstrated that dust particles indeed could crystallize in the vertical direction. A natural next step of these investigations is to have a detailed study of the crystalline structure, which is impractical for Monte Carlo simulation due to severe numerical limitations.

In this paper we report on a theoretical study of the phase diagram of plasma crystals. As a practical computational method we choose to incorporate the actions of the *microscopic* gravitational and drag forces by an effective dipole-dipole interaction that modifies the dominant monopole-monopole interaction that acts among dust particles placed on a lattice and focus on the system's *macroscopic* phase structure. We show that, under conditions that appear to be consistent with the experiments, a dipole-dipole interaction as weak as that which may be induced by gravity alone already plays a decisive role in the phase diagram. At first sight it may seem surprising that gravity could have such an effect on a structure mainly dictated by electromagnetism. This turns out to be the combined effect of several causes: the size of the mesoscopic dust particles is just about right for gravity to begin to compete with electromagnetism; near stability the energy difference between different crystal structures typically is just a minute fraction of the potential energy; Debye screening enhances the effect of the dipole-dipole interaction. The demand for accuracy is reflected in the size of the lattice used in the computation, which is typically $(30/a)^3$, where a is the lattice spacing in units of the Debye length.

The rotational invariance breaking dipole-dipole interaction is induced by the drag force as well as by gravity, but, owing to large theoretical and experimental uncertainties, it is not clear which (or if any) one of them is the dominant agent. At the end of this paper we propose an experiment to discriminate between the two possibilities.

CHARGING OF DUST PARTICLES AND DEBYE SCREENING

The basic force between (the dust) particles is screened Coulomb repulsion. An order of magnitude estimate of the charge carried by a particle is $Q = C\Delta\phi \approx 4\pi\epsilon_0 r_P \Delta\phi$, where C is the capacitance of basically a sphere of radius r_P. The potential difference $\Delta\phi$ between the surface of the particle and the plasma is obtained [12] by equating the thermal electron and ion currents toward the dust particle. This method was found to be not very accurate in experiment [4] and might underestimate the charge. More accurate estimates can be made by solving Poisson-Vlasov equations under certain assumptions [13] or may be obtained from independent experiments [4].

At distances large enough compared to particles size r_P,

the Coulomb force in the plasma is effectively screened to become a Yukawa potential whose range is given by the Debye length λ, with $\lambda^{-1} = [(e^2/4\pi\epsilon_0)(n_e/kT_e + n_i/kT_i)]^{1/2} \approx (n_i e^2/4\pi\epsilon_0 kT_i)^{1/2}$. This estimate can be improved [13]. Experimentally [1,4,3,2] r_P varies from a fraction of a micrometer to several tens of micrometers; Q is estimated or measured to be about 10^3-10^5 electron charges; T_e is a few eV; T_i is essentially room temperature; $n_e \approx n_i$, sensitive to the rf power, are of order 10^9-10^{10} cm^{-3}. The important fact is that in all plasma crystal experiments the interparticle distance $\bar{a} \equiv n_P^{-1/3}$, with the particle density n_P being of order 10^4-10^5 cm^{-3}, is a few tens to hundreds of micrometers and is larger than λ. We will assume that the particles reach thermal equilibrium with the ions and neutral atoms at room temperature [14] and ignore the fact that at very large distances the potential may decay even faster than the Yukawa potential.

We will use λ as the unit of length and $Q^2/4\pi\epsilon_0\lambda$ as the unit of energy. In these units the screened (Yukawa) potential is $V(r) = \exp(-r)/r$ and $a \equiv \bar{a}/\lambda$ is a number varying from about 2 to 10. The dusty plasma therefore resembles a hard-sphere system or a metal more than it resembles a classical Coulomb system.

INDUCED DIPOLE-DIPOLE INTERACTION

Consider a particle suspended in the bulk of the crystal away from the vertical walls of the containing vessel. Its suspension implies the presence of an approximately constant electric field E balancing the gravity force:

$$Mg + F_{\text{drag}} = QE, \tag{1}$$

where $M = (4\pi/3)r_P^3\rho$ is the mass of a spherical particle with density ρ. The combined electric, gravitational, and drag forces will keep the center of gravity of the particle at rest, but the electric field will still induce an electric-dipole moment on the charge distribution on the particle [15]. A simple approximation for the polarizability $P \approx 4\pi\epsilon_0 r_P^3$ yields a dipole moment $d \approx 4\pi\epsilon_0 r_P^3 E$. In the case $F_{\text{drag}} = 0$, the ratio of the strength of the dipole-dipole interaction to the monopole Yukawa interaction is

$$D = (d/Q\lambda)^2 \approx (4\pi r_P^6 \rho g e/3Q^2)^2 (4\pi\epsilon_0 n_e/kT_i) \equiv V_D n_e. \tag{2}$$

Here the volume V_D is defined to highlight the dependence of D on n_e. This rough estimate brings out an important point: D grows very rapidly, certainly faster than Q does, with increasing r_P. The drag force is difficult to estimate quantitatively [9,10]. In what follows we will not discuss it explicitly except to point out that the effect of its presence is to increase the value of D. The set of values $n_e = 10^9$ cm^{-3}, $r_P = 5$ μm, $\rho = 3$ g cm^{-3}, $Q = 1000$, and $kT_i = 300$ K yields $D = 0.0042$. Typical experimental values [1,4,3,2] are such that D ranges from less than 0.001 to a few times 0.1. It will be shown that the phases of the dusty plasma is effected when D is as small as 0.001 and that triangular phases begin to occur within the $D \sim 0.02-0.1$ range. The mesoscopic size of $r_P \approx 5$ μm seems to be just right for the interface of gravity with electromagnetism to be interesting.

The dipoles influence the crystal properties via interactions of dipole-monopole and dipole-dipole type. In a region where the charge and dipole moment carried by the particles are uniform the monopole-dipole interactions cancel exactly. We shall assume this to be the case and also ignore finite-size effects. Then the major effect on the crystal structure produced by dipoles is the screened dipole-dipole interaction $U(\vec{r}) = -D\partial^2/\partial z^2 V(r)$, which, together with the monopole-monopole Yukawa interaction, is

$$v(\vec{r}) = V(r) + U(\vec{r})$$
$$= [1 - D\{z^2/r^2 + (2z^2-u^2)(1/r^3+1/r^4)\}]e^{-r}/r, \tag{3}$$

where $u^2 \equiv r^2 - z^2 = x^2 + y^2$. By examining U one sees that it is attractive between two nearest neighbors in the z direction and repulsive in the x-y plane. For $r > 1$, which is true when the interparticle distance is greater than the Debye length, the leading terms, those with $1/r^2$ and $1/r^3$ dependences, come from screening. That is, the effect of the dipole-dipole interaction is enhanced by screening.

LATTICES

In the absence of dipole interactions, that is, when $D = 0$, (the energy of) the crystal is invariant under three-dimensional (3D) rotations and one needs to consider only four type of lattices: the cubic fcc (hereafter denoted by F), the cubic bcc B, the triangular hcp, and the 2D hexagonal. When $D \neq 0$, the lattices are deformed so that a reclassification is needed. For the deformed B and F we define two types of orthorhombic lattices: $R2$, composed of two rectangular sublattices whose coordinates for the lattice sites in units of the spacing a_x are $(x,y,z) = (l,m/g_\parallel,k/g_\perp)$ and $(x',y',z') = [l+1/2,(m+1/2)/g_\parallel,(k+1/2)/g_\perp]$; and $Rh2$, composed of two ''diamond'' sublattices with coordinates $(x,y,z) = (l+m/2,m/2g_\parallel,k/g_\perp)$ and $(x',y',z') = [l+m/2 +1/2,m/2g_\parallel,(k+1/2)/g_\perp]$; $g_\parallel$ and $g_\perp$ are aspect ratios in the x-y plane and the z direction, respectively, and l,m,k are integers. The $R2$ lattice with $(g_\parallel,g_\perp) = (1,1),(1,1/\sqrt{2})$, $(1/\sqrt{2},1)$ corresponds to $B100$ [i.e., bcc(100)], $F100$, and $F110$, respectively, and the $Rh2$ lattice with $(g_\parallel,g_\perp) = (1,1/\sqrt{2}),(1/\sqrt{2},1/\sqrt{2}),(1,1)$ corresponds to $B100$, $B110$, and $F100$, respectively. We call the deformed triangular 2D hexagonal, hcp, and $F111$ lattices $T1$, $T2$, and $T3$, respectively. The general trend of the effect of the dipole interaction on shape is to flatten the lattice in the z direction and, in the case of $R2$ and $Rh2$, elongate it in the y direction; the triangles, which for symmetry reasons always lie in the x-y plane, are extremely robust against deformation. In what follows, we use $R2$ and $Rh2$ specifically to indicate significantly deformed $F110$ and $B110$, respectively. For notational simplicity, we refer to the aspect ratio(s) of a lattice (collectively) as g.

METHOD OF CALCULATION OF THE PHASE DIAGRAM

In the calculation of the ground-state energy the following lattice sums are needed:

$$\epsilon \equiv \sum_{\mu \neq 0} v(\vec{R}_\mu), \quad \Sigma_x \equiv \sum_{\mu \neq 0} \partial^2/\partial x^2 v(\vec{R}_\mu),$$

$$\Sigma_z \equiv \sum_{\mu \neq 0} \partial^2/\partial z^2 v(\vec{R}_\mu), \qquad (4)$$

where μ denotes a lattice site and $\vec{R}_\mu$ is its position relative to the origin $\vec{R}_0 = 0$. Since $\vec{R}_\mu$ depends on the aspect ratio, these quantities are implicit functions of g. At zero temperature the ground-state energy per particle is just $\epsilon(g)$.

At finite temperatures we use the mean-field approximation and the Lindemann criterion. The criterion expresses the critical value for the root-mean-squared deviation of a particle from its stable lattice site as $[\langle(\Delta x)^2\rangle_C]^{1/2} = c_L a$. For Yukawa crystals, molecular-dynamics simulations yield the essentially a-independent value of $c_L = 0.16 - 0.19$ for the melting curve (in the range $a \sim 1$–10) [16–19]. For $D \neq 0$, molecular-dynamics simulations would also be a better method than mean-field theory for an accurate determination of the melting curve. However, a judicious application of the Lindemann criterion for melting suffices for our purpose since one does not expect the small dipole effect to significantly change the melting line.

For any crystal structure, one expects mean-field theory, which misses out on some soft modes, to yield a smaller effective value for the Lindemann coefficient for a similar melting phenomenon [20]. Using the Einstein approximation, we reproduce the melting curve of molecular-dynamics simulations at $D = 0$ with the value $c_L^{\text{eff}} = 0.054$. This is the value we use for the Lindemann coefficient throughout.

In the Einstein approximation [21,20], the mean-field potential energy at a point $\vec{r}$ near the lattice site $\vec{R}_0 = 0$ is

$$\langle e(\vec{r})\rangle = \sum_{\mu \neq 0} \langle v(\vec{R}_\mu - \vec{r})\rangle$$
$$= \epsilon + (1/2)[(2\xi_x^2 + u^2)\Sigma_x + (\xi_z^2 + z^2)\Sigma_z], \qquad (5)$$

where $\langle O(\vec{r})\rangle = \int \Pi_{i=1}^3 [dx_i'(2\pi)^{-1/2}\xi_i^{-1}\exp(-x_i'^2/2\xi_i^2)]O(\vec{r}-\vec{r}')$ and we have taken the thermal fluctuations lengths $\xi_x = \xi_y$ for simplicity. The same distribution function yields $\xi_x^2\Sigma_x = \xi_z^2\Sigma_z = T$. The free energy per particle for a given aspect ratio g is

$$F = T\ln\left(\int d^3r \exp[-\beta\langle e(\vec{r})\rangle]\right) - 1/2\langle e(0)\rangle$$
$$= (1/2)(\epsilon + 3T/2) + (T/2)\ln\{[(2\pi)^3 T^3]/\Sigma_x^2\Sigma_z\} \qquad (6)$$

In actual computations, the value(s) of g is (are) determined numerically by minimizing the free energy and a lattice size of $(30/a)^3$ seems to produce the required accuracy. Some results are shown in Figs. 1 and 2. Details of our calculations are presented elsewhere [22].

DISCUSSION OF RESULTS AND CONCLUSIONS

In Fig. 1 the phase diagram is given as a function of D and a at zero temperature. The well-known B-F transition at $a = 1.73$ [21,20,16] is indicated, although even for D as small as 0.001 there are already preferred orientations. For $a > 4$ the dipole effect is so weak that the various orientations of the F lattice are practically degenerate with $D < 0.01$, beyond
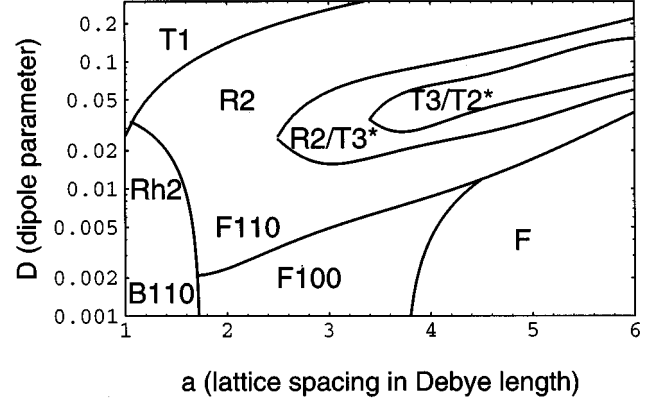

FIG. 1. Phase diagram as a function of the dipole parameter D and lattice spacing a at zero temperature.

which the phase diagram becomes more complex. As the lattices become increasingly deformed by the dipole interaction, it becomes necessary to label the $B110$ lattice as $Rh2$, $F110$ as $R2$, $F111$ as $T3$, and so on. For $Rh2$, the effect of deformation on the aspect ratios never exceeds a few percent. For $R2$ the effect can be large. For example, for $a = 2$, $(g_\parallel, g_\perp)$ is (0.697, 1.04) at $D = 0.02$ and it is (0.607, 1.30) at $D = 0.1$. There is a narrow strip in the upper-right corner of the phase diagram where $T3$ is stable and where $T2$ is almost degenerate with $T3$ (energies are within one part in 10^5) and a larger strip where $T3$ is almost degenerate with $R2$. When uncertainties or distributions in the values of the parameters of the system are taken into account, one expects the $R2$, $T2$, and $T3$ to co-exist in the general area.

The phase diagram is dominated by $R2$ and $T1$ above the line $D \approx -0.024 + 0.054a$. When D is greater than the critical value given by $D_c = -0.861 + 0.111a + 0.0128a^2$, indicated by the $R2 \rightarrow T1$ transition line in Fig. 1, $g_\parallel$ for $R2$ takes the critical value $\sqrt{1/3}$ (at this value the 2D projections of $R2$ and $T1$ are identical) and $R2$ and $T1$ simultaneously collapse vertically to become the same 2D hexagonal lattice *within our model*, where the dust particles are represented by points. In practice, two particles are strongly repulsed by the unscreened Coulomb force when they are separated by less than one Debye length. Therefore, when a lattice vertically collapses in our model, we take it to indicate that the actual vertical separation of the horizontal two-dimensional sublattice is about one Debye length, regardless of the value of a. We call this a "collapsed" $T1$ state; it occupies the upper-left-hand corner of Fig. 1. The critical value for vertical aspect ratio is $g_\perp \approx 2.177 - 0.112a$.

These features are not changed much at finite temperature. In all cases the solid to liquid curve is approximately given by the line $T^* \approx 0.04a - 0.03$, where $T^* = kT/V(a)$ is a universal dimensionless scaled temperature.

In experiments certain parameters such as the rf power are varied, while others are kept fixed. In particular the dust particle temperature is fixed at $T = T_i = 300$ K. To roughly simulate a laboratory setting, we take $V_D = 2 \times 10^{11}$ cm^3 and let $n_{e0} \equiv n_e/10^9$ cm^{-3} and $n_{p0} \equiv n_P/10^5$ cm^{-3} range from 0.2 to 20 and 0.1 to 10, respectively. Then $D \approx 0.02n_{e0}$, $\lambda_0 \approx (2/n_{e0})^{1/2}$, $a \approx 1.52n_{e0}^{1/2}n_{P0}^{-1/3}$, and the dimensionless temperature $T^* \approx 4.31 \times 10^{-4} n_{P0}^{-1/3} e^a$. The calculated phase diagram is shown in Fig. 2 in a $\log n_p \log n_e$ plot. No result is
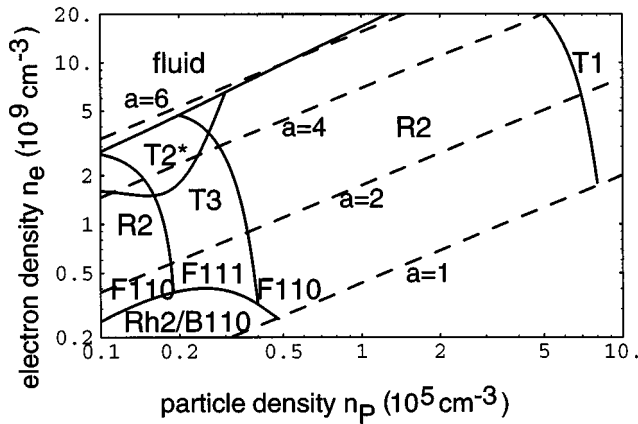
FIG. 2. Phase diagram as a function of electron and particle densities for $V_D = 2 \times 10^{11}$ cm^3 or $D \approx 0.02 n_e/10^9$ cm^{-3}. Temperature is fixed at room temperature and dashed lines are lines of constant lattice spacing.

given for $a < 1$, where the model is not reliable.

The melting line is approximately given by $T_m^* = 0.2$. In terms of the dimensionless coupling strength $\Gamma = Q^2 V(r_0/\lambda)/4\pi\epsilon_0 r_0 kT$, where $r_0 = (3/4\pi n_P)^{1/3}$ is the Wigner-Seitz radius of the dust particles, the melting temperature corresponds to a strength of $\Gamma_m \approx 70 \pm 10$, similar to the value ≈ 67 obtained in [20] for colloidal suspensions. In a typical experiment [1], n_P is fixed and n_e is varied indirectly by varying the rf power. The phase diagram indicates that turning up the rf power, which will cause n_e to increase, will eventually cause melting. This seems to agree with experiment [1]. Note that even as T is kept unchanged, increasing n_e increases λ and consequently T^*. The phase diagram in the region $n_P \lesssim 0.5$ is relatively complex, with four lattices occupying five domains. Whereas transitions such as $R2 \rightarrow T3$ are real phase transitions, changes such as $B110 \rightarrow Rh2$ and $F110 \rightarrow R2$ are crossovers. Strictly speaking, there is a second-order phase transition whenever F bifurcates to two oriented F-type lattices. As complex as it has made the phase diagram in this region, the dipole interaction changes the aspect ratio from its $D=0$ value by less than 4%. In the domain marked by $T2^*$, $T2$ has the second lowest energy, but its energy is greater than the energies of the stable phases by less than a few parts in 10^5. In fact, in this region the energies of $Rh2$, $R2$, $T3$, and $T2$ are all within a fraction 10^{-4} of each other. Given that the experimental val-

ues of n_e and n_P have a non-negligible spread, we expect these phases to coexist in a typical experimental setting.

The region $0.5 \gtrsim n_P \gtrsim 6$ is dominated by $R2$, whose energy is lower than those of $T2$ and $T3$ by more than 0.03% when $n_P > 2$. Here $R2$ typically has aspect ratios ($0.58 \gtrsim g_\parallel \gtrsim 0.68$, $1.1 \lesssim g_\perp \lesssim 1.5$) that renders it no longer recognizable as a deformation of $F110$. The upper-right-hand corner of the phase diagram is occupied by the collapsed $T1$ state explained earlier, which typically has $g_\perp \gtrsim 1.7$. In comparison, our computation shows that a quasi-2D lattice of several layers (not surprisingly) may have an uncollapsed stable $T1$ structure. In particular, with five layers, the phase diagram in the region $2 \leq a \leq 4$ is occupied by $T1$ with $1.5 \gtrsim g_\perp \gtrsim 1.2$ and in the region $4 < a \leq 6$ has two phases: $R2$ below the line $D \approx 0.616 - 0.271/(a-3.6)$ and $T1$ above and along which $1.2 \gtrsim g_\perp \gtrsim 1.6$ for $T1$.

In summary, our study suggests that the induced electric-dipole interaction, whose strength is a rapidly increasing function of the dust particle size, can explain the crystalline phases of the dusty plasma seen in experiments. The presence of the dipole interaction is first manifest in the preferred orientation of the cubic lattices. At intermediate dipole strength, the triangular lattices $T3$ and $T2$ (deformed $F111$ and hcp, respectively) begin to coexist with the preferred cubic lattice $R2$ ($F110$). At higher dipole strength the vertically collapsed hexagonal $T1$ is the stable phase. The question remains as to whether gravity or the drag force is mainly responsible for the dipole-dipole interaction. At the moment this question cannot be clearly resolved experimentally because in all the experiments reported so far the direction of gravity coincides with that of the ion stream. It seems that in an experiment in which the chamber holding the plasma is tilted, thereby making the directions of the two forces different, one would be able to disentangle the effects of the two forces.

[1] J.H. Chu and Lin I, Phys. Rev. Lett. **72**, 4009 (1994); I. Lin et al., Chin. J. Phys. **33**, 453 (1995).
[2] Y. Hayashi and K. Tachibana, Jpn. J. Appl. Phys. **33**, 804 (1994).
[3] H. Thomas et al., Phys. Rev. Lett. **73**, 652 (1994).
[4] A. Melzer et al., Phys. Lett. A **191**, 301 (1994).
[5] Y. Hayashi and K. Tachibana, J. Vac. Sci. Technol. A **14**, 506 (1996).
[6] J.B. Pieper et al., J. Vac. Sci. Technol. A **14**, 519 (1996).
[7] H. Ikezi, Phys. Fluids **29**, 1764 (1986).
[8] J.P. Hansen, Phys. Rev. A **8**, 3096 (1973).
[9] S. Vladimirov and M. Nambu, Phys. Rev. E **52**, R2172 (1995).
[10] F. Melandso and J. Goree, J. Vac. Sci. Technol. A **14**, 511 (1996).
[11] A. Melzer et al., Phys. Rev. E **54**, R46 (1996); E.L. Pollock and J.P. Hansen, Phys. Rev. A **8**, 3110 (1973).
[12] M.S. Barnes et al., Phys. Rev. Lett. **68**, 313 (1992).
[13] J.E. Daugherty et al., Appl. Phys. **72**, 3934 (1992).
[14] J.E. Daugherty et al., J. Appl. Phys. **73**, 1617 (1993).
[15] J.E. Daugherty et al., J. Appl. Phys. **73**, 7195 (1993).
[16] M.O. Robbins et al., J. Chem. Phys. **88**, 3286 (1988); M.J. Stevens and M.O. Robbins, ibid. **98**, 2319 (1993).
[17] E.J. Meijer and D. Frenkel, J. Chem. Phys. **94**, 2269 (1991).
[18] R.T. Farouki and S. Hamaguchi, Appl. Phys. Lett. **61**, 2973 (1992); J. Chem. Phys. **101**, 9885 (1994); S. Hamaguchi and R.T. Farouki, ibid. **101**, 9876 (1994).
[19] Y. Rosenfeld, J. Chem. Phys. **103**, 9803 (1995).
[20] R.O. Rosenberg and D. Thirumalai, Phys. Rev. A **36**, 5690 (1987).
[21] D. Hone et al., J. Chem. Phys. **79**, 1474 (1983)
[22] H.C. Lee and B. Rosenstein (unpublished).